ENVIRONMENTAL RESEARCH
LETTERS

LETTER • **OPEN ACCESS**

Pronounced inter-model uncertainties in TRENDY-simulated terrestrial carbon sink responses to hydroclimatic extremes

To cite this article: Zishan Wang *et al* 2026 *Environ. Res. Lett.* **21** 054021

ENVIRONMENTAL RESEARCH
LETTERS

OPEN ACCESS

RECEIVED
1 December 2025

REVISED
3 February 2026

ACCEPTED FOR PUBLICATION
27 February 2026

PUBLISHED
10 March 2026

LETTER

Pronounced inter-model uncertainties in TRENDY-simulated terrestrial carbon sink responses to hydroclimatic extremes

Zishan Wang[1,2], Jun Wang[1,2,*], Benjamin Poulter[3], Gesa Meyer[4], George Hurtt[5], Hao Zhou[6], Lei Ma[5], Patrick C McGuire[7], Qing Sun[8,9], Wenping Yuan[10] and Xiaoni Wang-Faivre[11]

[1] International Institute for Earth System Science, Nanjing University, Nanjing, Jiangsu, People's Republic of China
[2] Jiangsu Provincial Key Laboratory of Geographic Information Science and Technology, Key Laboratory for Land Satellite Remote Sensing Applications of Ministry of Natural Resources, School of Geography and Ocean Science, Nanjing University, Nanjing, Jiangsu, People's Republic of China
[3] Spark Climate Solutions, San Francisco, CA, United States of America
[4] Climate Research Division, Environment and Climate Change Canada, Victoria, British Columbia, Canada
[5] Department of Geographical Sciences, University of Maryland, College Park, MD, United States of America
[6] College of Meteorology and Oceanography, National University of Defense Technology, Changsha, People's Republic of China
[7] Department of Meteorology and National Centre for Atmospheric Science (NCAS), University of Reading, Reading, United Kingdom
[8] Oeschger Centre for Climate Change Research, University of Bern, Bern, Switzerland
[9] Climate and Environmental Physics, Physics Institute, University of Bern, Bern, Switzerland
[10] Institute of Carbon Neutrality, Sino-French Institute for Earth System Science, College of Urban and Environmental Sciences, Peking University, Beijing, People's Republic of China
[11] LSCE, Paris, France
[*] Author to whom any correspondence should be addressed.

E-mail: wangjun@nju.edu.cn

Keywords: hydroclimatic extremes, terrestrial carbon sink responses, inter-model uncertainties, TRENDY models, FLUXNET observations

Supplementary material for this article is available online

Abstract

Hydroclimatic extremes are critical regulators of terrestrial carbon sink dynamics, yet their representation in terrestrial biosphere models remains highly uncertain. Here, we assessed uncertainties in Trends in Net Land-Atmosphere Exchange (TRENDY) v12 model simulations of carbon sink responses to hydroclimatic extremes during 1980–2022 by systematically comparing model outputs across regions, event types, and biomes. Site-level evaluations reveal that the multi-model ensemble mean correctly captures the sign of net biome productivity (NBP) anomalies at approximately 60% of stations; however, while the multi-model ensemble mean generally replicates NBP variations during dry events, its performance degrades during wet events. Spatially, most regions act as anomalous carbon sinks during wet extremes, a pattern that largely reverses during dry events. Despite these general trends, substantial inter-model heterogeneity persists. Inter-model uncertainties are more pronounced under dry events between 30° S and 30° N, while other latitudes exhibit comparable or even greater spreads under wet events. Specifically, inter-model spread is more sensitive to wet anomalies in arid and semi-arid regions, but to drought-induced stress in semi-humid and humid regions. Across biomes, uncertainties are greater for grasslands, savannas, and shrublands during wet events, shifting to forests and croplands during dry events. Finally, we demonstrate that the divergent NBP responses primarily originate from uncertainties in simulating gross primary production. Our findings highlight the persistent challenges TRENDY models face in capturing ecosystem responses to hydroclimatic extremes, underscoring the urgent need to improve simulation fidelity in a rapidly changing climate.

1. Introduction

The terrestrial biosphere plays a critical role in regulating the global carbon cycle by serving as a natural sink for anthropogenic CO_2 emissions from fossil fuel combustion and land-use and land-cover change (Sitch *et al* 2024). Since the 1960s, terrestrial ecosystems have absorbed roughly one-third of annual anthropogenic emissions, thereby mitigating the pace of climate change (Friedlingstein *et al* 2025), albeit with substantial interannual variability (Wang *et al* 2018, He *et al* 2022). However, the increasing frequency and intensity of climate extremes threaten the stability of this land carbon sink (Piao *et al* 2019). Drought is widely recognized as a dominant climate stressor, reducing vegetation productivity and strongly regulating ecosystem respiration across regional to global scales (Xu *et al* 2012, Zscheischler *et al* 2014a, Von Buttlar *et al* 2018, Wang *et al* 2023, Yan *et al* 2024). In contrast, although emerging evidence shows that precipitation extremes can substantially alter carbon fluxes, their impacts vary seasonally and depend on antecedent soil water content (Fay *et al* 2011, Zeppel *et al* 2014). Despite their importance, systematic assessments of how precipitation extremes influence terrestrial carbon dynamics remain limited.

Terrestrial biosphere models (TBMs) have been widely used to investigate ecosystem responses to hydroclimatic extremes. A global-scale analysis of 10 state-of-the-art terrestrial carbon models from the North American Carbon Program Multi-scale Synthesis and Terrestrial Model Intercomparison Project revealed that droughts substantially reduce gross primary production (GPP) and, to a lesser extent, total respiration, whereas wet periods exert a smaller, opposite effect (Zscheischler *et al* 2014b). Projections from the Coupled Model Intercomparison Project Phase 6 suggest that GPP will decline in most regions under future drought intensification under different shared socioeconomic pathways, with the strongest reductions expected in low- and mid-latitudes (Chen *et al* 2025). Extreme droughts are projected to exert the most pronounced impacts on GPP by the end of the century, surpassing those of moderate or severe droughts. Simulations from the Inter-Sectoral Impact Model Intercomparison Project phase 2a also show reductions in net primary production and heterotrophic respiration (Rh) during extreme dry events (Pan *et al* 2020). In contrast, a semi-empirical physical model developed by Zhang *et al* (2025) revealed that medium and heavy precipitation events can trigger longer-lasting and more intense responses of net ecosystem carbon exchange (NEE). Consistently, the weakening of terrestrial carbon sinks following extreme summer precipitation has been captured by both Vegetation-Global Atmosphere–Soil and Lund–Potsdam–Jena-Wald, Schnee, Landschaft simulations, although the magnitude of the reduction varies among models (Wang *et al* 2026). Despite these advances, substantial uncertainties persist, characterized by frequent model divergence in ecosystem response representations and poor alignment with observations (Seiler *et al* 2022).

Every year, the state-of-the-art TBMs participating in the Trends in Net Land-Atmosphere Exchange (TRENDY) provide the land carbon sink estimates for the Global Carbon Project (Friedlingstein *et al* 2025). TRENDY simulations demonstrate considerable proficiency in capturing global vegetation biomass, GPP, and ecosystem respiration across both annual and long-term timescales (Seiler *et al* 2022, Dai *et al* 2024), establishing them as a robust framework for evaluating ecosystem responses to climate variability. However, the extent to which these models consistently represent carbon flux responses to hydroclimatic extremes remains unclear. Here, we assess the divergence in TRENDY model simulations of terrestrial carbon cycle responses to extreme wet and dry events by systematically comparing model outputs across regions and event types. We aim to identify emergent signals, quantify inter-model uncertainty, and provide insights into the reliability of current TBMs in capturing the impacts of hydroclimatic extremes on the land carbon sink.

2. Materials and methods

2.1. Eddy covariance (EC) observations

Monthly GPP, total ecosystem respiration (Reco), and NEE data were obtained from 34 EC sites within the FLUXNET 2015 dataset, each featuring long-term records ($\geqslant$8 years) and more than one occurrence of wet or dry events as per our defined criteria. These data were used to evaluate vegetation-specific responses to hydroclimatic events. The EC technique captures dynamic variations in ecosystem production, respiration and net carbon exchange through continuous, high-frequency, and automated observations at the ecosystem scale (Yu *et al* 2013, Pastorello *et al* 2020, Jiao *et al* 2024). In this study, GPP and Reco estimates were derived using the standardized daytime partitioning method (GPP_DT_VUT_REF and RECO_DT_VUT_REF) (Pastorello *et al* 2020).

Vegetation at these sites was categorized according to the International Geosphere–Biosphere Program (IGBP) scheme (Loveland and Belward 1997). Site-specific details are provided in table S1. For global-scale analysis, land cover was defined using the Moderate Resolution Imaging Spectroradiometer Land Cover Type (MCD12Q1) Version 6.1 (Friedl and Sulla-Menashe 2022), which aligned with the site-level IGBP standards. Both EC sites and model

simulations were grouped into broad functional types as follows: forest (ENF + DBF + EBF + MF), grassland, cropland (CRO + CVM), wetland (WET), shrubland (OSH + CSH), and savanna (SAV + WSA). Further, the forest category was partitioned into tropical and extra-tropical forests using the Köppen–Geiger climate classification system, following the methodology of Ahlström *et al* (2015).

2.2. TRENDY v12 multi-model simulations

We utilized outputs from state-of-the-art TBMs provided by the TRENDY project. The TRENDY project comprises three main experimental protocols: S1 (dynamic CO_2 only), S2 (dynamic CO_2 and climate), and S3 (dynamic CO_2, climate, and land use) (Sitch *et al* 2015). The S3 simulation from TRENDY v12 was employed in this study for the period 1980–2022. Models incorporating GPP, NBP, autotrophic respiration (Ra), and heterotrophic respiration (Rh) were retained for analysis, whereas those with insufficient temporal coverage or coarse spatial resolution were excluded. The term 'Reco' in this study denotes the total ecosystem respiration, calculated by the sum of Ra and Rh. In detail, the 15 TBMs used here include CABLEPOP (Haverd *et al* 2018), CLASSIC (Asaadi *et al* 2018, Melton *et al* 2020), CLM5.0 (Lawrence *et al* 2019), ELM (Burrows *et al* 2020, Yang *et al* 2023), EDv3 (Moorcroft *et al* 2001, Ma *et al* 2022), IBIS (Yuan *et al* 2014), ISAM (Jain *et al* 2013, Meiyappan *et al* 2015, Shu *et al* 2020), ISBACTRIP (Delire *et al* 2020), LPJwsl (Poulter *et al* 2011), LPX-Bern (Lienert and Joos 2018), OCN (Zaehle and Friend 2010, Zaehle *et al* 2011), ORCHIDEE (Krinner *et al* 2005, Zaehle and Friend 2010, Vuichard *et al* 2019), SDGVM (Woodward and Lomas 2004, Walker *et al* 2017), VISIT (Ito and Inatomi 2012, Kato *et al* 2013), and YIBs (Yue and Unger 2015). Table 1 summarizes the land carbon components and native horizontal spatial resolutions of the selected models. Considering the varying horizontal resolutions across TBMs, all relevant monthly variables were interpolated to a 0.5° × 0.5° spatial resolution consistently.

2.3. Meteorological data

Monthly precipitation data were obtained from the Climatic Research Unit Time-Series (CRU TS 4.09) with a spatial resolution of 0.5° × 0.5° for the 1980–2022 period, one of the most widely used climate datasets globally developed by the National Centre for Atmospheric Science. Based on long-term precipitation data, the 3 month Standardized Precipitation Index (SPI-3) was calculated to identify extreme hydroclimatic events. Established from a gamma distribution fitted to historical monthly precipitation totals, the SPI was computed by transforming the cumulative probability of precipitation into a standard normal distribution. This index is used to monitor precipitation anomalies and serves as a proxy for the impacts of heavy rainfall and droughts (Thi *et al* 2023, Steensen *et al* 2025). The calculation of SPI values is based on equation (1), as below:

$$SPI = \begin{cases} \left(k - \frac{c_0 + c_1 k + c_2 k^2}{1 + d_1 k + d_2 k^2 + d_3 k^3}\right), & 0.5 < H \leq 1 \\ -\left(k - \frac{c_0 + c_1 k + c_2 k^2}{1 + d_1 k + d_2 k^2 + d_3 k^3}\right), & 0 < H \leq 0.5 \end{cases} \quad (1)$$

where $k = \sqrt{\ln\left(\frac{1}{(1-H)^2}\right)}$ or $k = \sqrt{\ln\left(\frac{1}{(H)^2}\right)}$, respectively, c_0, c_1, c_2, d_1, d_2 and d_3 are coefficients and H is the gamma function (Mckee *et al* 1993, Lloyd-Hughes and Saunders 2002). SPI values were calculated using monthly precipitation data from CRU (1980–2022) with the Climate Indices Python package (Adams 2017).

In addition, the multi-year average annual precipitation was calculated to facilitate the classification of regions into four precipitation categories in subsequent analyses: arid (<200 mm), semi-arid (200–400 mm), semi-humid (400–800 mm), and humid (>800 mm) (Huang *et al* 2021).

2.4. Definitions of hydroclimatic events

In this study, hydroclimatic extremes were primarily identified using the SPI-3, supplemented by precipitation-based thresholds for robustness. According to the SPI classification (table 2; Rhee and Im 2017), extreme wet and extreme dry conditions were defined as monthly SPI-3 values >2.0 and <−2.0, respectively. For site-level analysis, events were identified when SPI-3 values exceeded these thresholds within each site's observational record.

To isolate the impacts of individual pulses and minimize legacy effects—consistent with the pulse–reserve paradigm (Feldman *et al* 2024)—we implemented a stringent selection criterion requiring the month preceding each event to exhibit near-normal conditions (−0.49 < SPI-3 < 0.49). Additionally, to ensure the findings were not index-dependent, extreme events were also defined using absolute precipitation thresholds: values exceeding the 95th percentile (wet) or falling below the 5th percentile (dry) of the long-term climatology.

2.5. Calculations of detrended anomalies

For both FLUXNET observations and TRENDY simulations, our analyses focused on detrended anomalies of NBP, GPP, and Reco. For each site or grid, seasonal cycles were first removed by subtracting the climatological monthly mean from the carbon flux time series (Yan *et al* 2023). Subsequently, linear trends were removed to account for long-term

Table 1. Terrestrial biosphere models (TBMs) used in this study.

Model	Spatial resolution	Time range	Variable	Reference
CABLEPOP	1° × 1°	1700–2022	GPP NBP Ra Rh	Haverd *et al* (2018)
CLASSIC	1° × 1°	1701–2022	GPP NBP Ra Rh	Asaadi *et al* (2018), Melton *et al* (2020)
CLM5.0	1.25° × 0.9424°	1701–2022	GPP NBP Ra Rh	Lawrence *et al* (2019)
ELM	1.25° × 0.9424°	1700–2022	GPP NBP Ra Rh	Burrows *et al* (2020), Yang *et al* (2023)
EDv3	0.5° × 0.5°	1700–2022	GPP NBP Ra Rh	Moorcroft *et al* (2001); Ma *et al* (2022)
IBIS	0.5° × 0.5°	1700–2022	GPP NBP Ra Rh	Yuan *et al* (2014)
ISAM	0.5° × 0.5°	1700–2022	GPP NBP Ra Rh	Jain *et al* (2013), Meiyappan *et al* (2015), Shu *et al* (2020)
ISBACTRIP	1° × 1°	1700–2022	GPP NBP Ra Rh	Delire *et al* (2020)
LPJwsl	0.5° × 0.5°	1700–2022	GPP NBP Ra Rh	Poulter *et al* (2011)
LPX-Bern	0.5° × 0.5°	1700–2022	GPP NBP Ra Rh	Lienert and Joos (2018)
OCN	1° × 1°	1700–2022	GPP NBP Ra Rh	Zaehle and Friend (2010), Zaehle *et al* (2011)
ORCHIDEE	0.5° × 0.5°	1700–2022	GPP NBP Ra Rh	Krinner *et al* (2005), Zaehle and Friend (2010), Vuichard *et al* (2019)
SDGVM	1° × 1°	1700–2022	GPP NBP Ra Rh	Woodward and Lomas (2004), Walker *et al* (2017)
VISIT	0.5° × 0.5°	1860–2022	GPP NBP Ra Rh	Ito and Inatomi (2012), Kato *et al* (2013)
YIBs	1° × 1°	1700–2022	GPP NBP Ra Rh	Yue and Unger (2015)

Table 2. Classification of hydroclimatic moisture regimes according to SPI.

Classification	SPI values
Extreme wet	⩾2.00
Severe wet	1.50 to 1.99
Moderate wet	1.00 to 1.49
Mild wet	0.50 to 0.99
Near normal	−0.49 to 0.49
Mild drought	−0.99 to −0.50
Moderate drought	−1.49 to −1.00
Severe drought	−1.99 to −1.50
Extreme drought	⩽−2.0

changes induced by drivers such as climate warming, CO_2 fertilization, and other external influences. This approach facilitated the isolation of short-term variations in carbon fluxes, enabling a clearer assessment of the immediate impacts of hydroclimatic extremes.

3. Results

3.1. Spatial responses of land carbon sink to hydroclimatic events

Given that the SPI-3 is a widely adopted metric for assessing short-term moisture conditions, we focused primarily on SPI-3-derived results, while analyses based on precipitation thresholds were included to verify the robustness of our findings. The latter exhibited spatial patterns that were largely consistent with the SPI-based results.

3.1.1. Site-level assessment of simulated carbon fluxes

We assessed variations in land carbon sink during hydroclimatic extremes by analyzing NBP anomalies from both FLUXNET observations and TRENDY v12 multi-model simulations. For the comparison, model outputs were extracted from the 0.5° × 0.5° grid cells containing each FLUXNET station. Our results indicate that the multi-model ensemble mean generally exhibits attenuated anomalous responses compared to observations (figures 1(a) and (d)). Specifically, while the multi-model ensemble mean reasonably captures site-level NBP variations during dry events ($R^2 = 0.31$, $p = 0.03$), this observation-model fidelity degrades significantly during wet events ($R^2 = 0.1$, $p = 0.17$). Despite these divergent magnitudes, the multi-model ensemble mean correctly reproduces the sign (positive or negative) of site-level NBP responses at approximately 60% of the stations across hydroclimatic extremes (64.7% for wet and 58.8% for dry, figure 1). Regional discrepancies further highlight model limitations. During extreme wet events, both datasets indicate negative anomalies in the eastern United States, albeit with differing magnitudes. In the northern Mediterranean, simulations exhibit

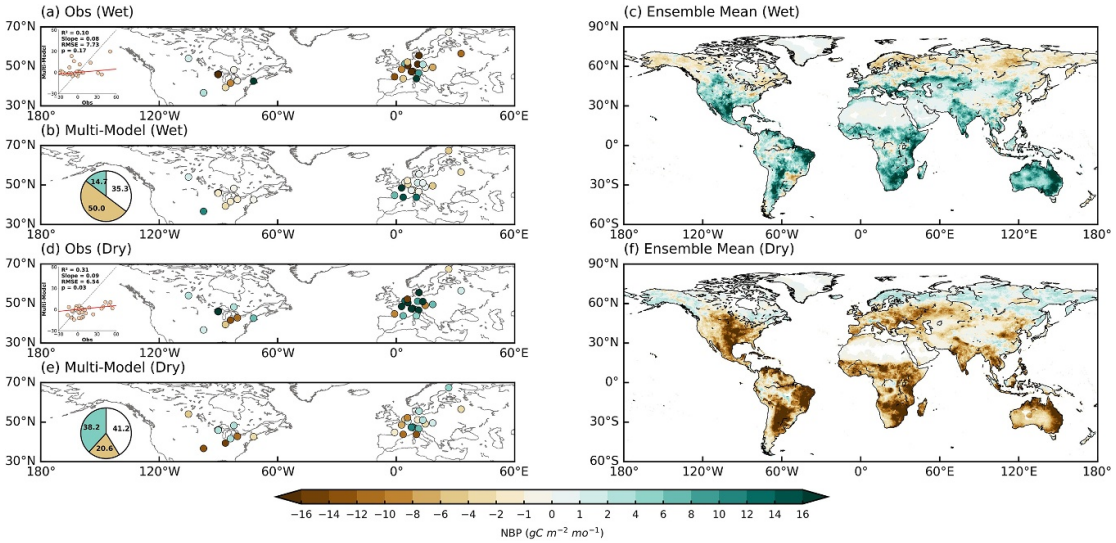

Figure 1. Detrended NBP anomalies under contrasting hydroclimatic events. Panels (a) and (d) show site-level NBP anomalies derived from FLUXNET during wet and dry events, respectively. Panels (b) and (e) present the multi-model ensemble mean NBP anomalies simulated by TRENDY v12 models, temporally aligned with the site observation periods. The inset scatter plots display the observed versus modeled NBP anomalies, along with R^2, slope, RMSE, and p-value. The inset pie charts illustrate the proportions of consistent positive (green), consistent negative (brown), and inconsistent signs (white) between observations and simulations. Panels (c) and (f) display the global multi-model ensemble mean NBP anomalies simulated by TRENDY v12 models across all wet and dry events from 1980 to 2022. NBP is expressed in gC m^{-2} mo^{-1}.

mixed signals, while station observations tend to produce strong negative anomalies (figures 1(a) and (b)). Conversely, during dry events, observations often suggest an enhanced carbon sink, especially in the northern Mediterranean where the simulations capture the signal well. These patterns persist when applying precipitation-based threshold criteria (figure S1).

3.1.2. Global patterns of simulated land carbon sink responses

Given the constrained temporal and spatial coverage of FLUXNET sites, we further examined the spatial patterns of simulated land carbon sink responses to wet and dry events (figures 1(c) and (f)). Under wet conditions, most regions act as anomalous carbon sinks (i.e. positive deviations from the long-term mean), with exceptions in high-latitude regions of the Northern Hemisphere (>50° N), the eastern United States, southeastern China, and southeastern South America (figure 1(c)). In contrast, the spatial distribution of NBP anomalies is nearly reversed during dry events (figure 1(f)). Results based on precipitation-defined thresholds show broadly consistent patterns, although both positive and negative anomalies are weaker in magnitude (figures S1(c) and (f)). Additionally, applying stringent event-filtering criteria produces more spatially dispersed NBP anomalies but does not alter the overall response, underscoring the robustness of these results (figures S2(c) and (f)).

3.2. Inter-model spread of responses to hydroclimatic extremes

We quantified the mean carbon flux anomalies for each individual model under contrasting hydroclimatic extremes. The inter-model spread was subsequently defined as the standard deviation across the multi-model ensemble, providing a measure of simulated uncertainty.

3.2.1. Global patterns

We then examined the inter-model spread of ecosystem responses to wet and dry events (figure 2). The spatial distribution of standard deviations across models reveals substantial heterogeneity under both hydroclimatic conditions, with pronounced spreads in the central United States, Europe, southeastern South America, most of Africa, northern and eastern Australia, and parts of South and East Asia (figures 2(a) and (b)). These results highlight the considerable uncertainties that current state-of-the-art TBMs still face in representing ecosystem responses to hydroclimatic extremes.

When comparing wet and dry conditions, the inter-model spread tends to be larger at high latitudes of the Northern Hemisphere, the southwestern United States, central Asia, and much of Australia during wet events, whereas greater uncertainties during dry events are concentrated in the low latitudes, Europe, and the central United States (figure 2(c)). Zonal averages further indicate that stronger inter-model spreads under dry events are primarily confined between 30° S and 30° N, while

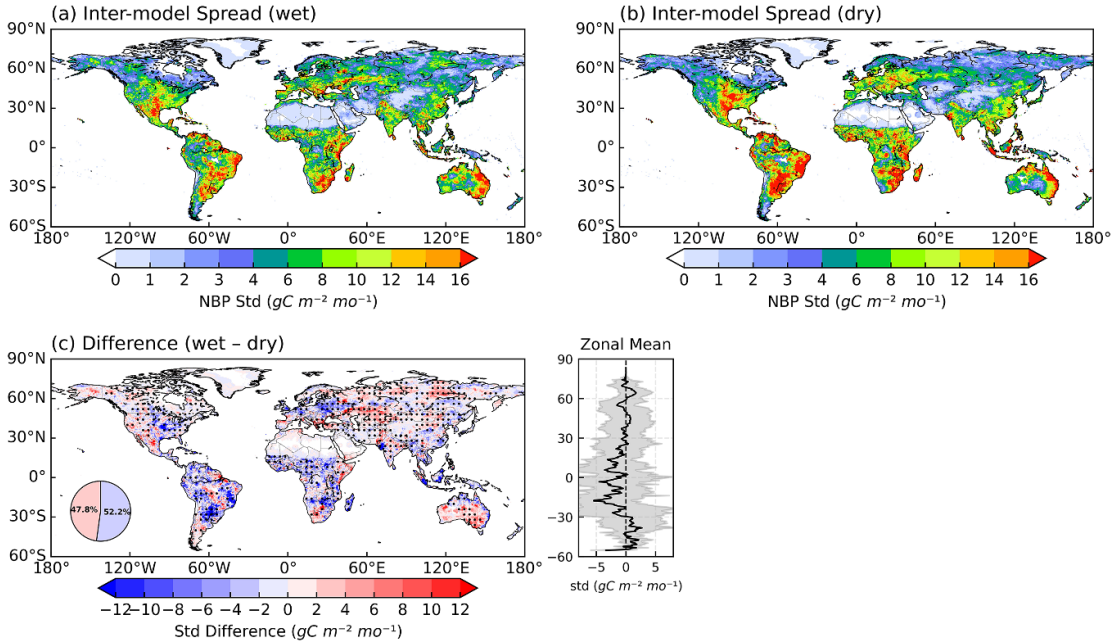

Figure 2. Inter-model spread in simulated NBP responses to hydroclimatic extremes. Panels (a) and (b) show the spatial distribution of inter-model spread (defined as the standard deviation) among TRENDY v12 models during wet and dry events, respectively. Panel (c) shows the differences in inter-model spread between wet and dry conditions, supplemented by the corresponding latitudinal averages. The inset pie chart demonstrates the percentage of vegetated areas exhibiting positive versus negative differences in spread. NBP is expressed in gC m^{-2} mo^{-1}. Regions marked with black dots indicate statistically significant differences based on the Levene's test ($p < 0.05$).

other latitudes exhibit comparable or even stronger spreads under wet events (figure 2(c)). Overall, inter-model uncertainty is nearly balanced between wet and dry conditions, with approximately 47.8% of vegetated areas exhibiting larger model spread under wet conditions and 52.2% under dry conditions. Results derived from precipitation-defined events display similar spatial patterns, albeit with weaker magnitudes (figure S3).

3.2.2. Uncertainties along the precipitation gradient

To better assess model uncertainties along precipitation gradient, we classified global land into four zones—arid, semi-arid, semi-humid, and humid—based on annual cumulative precipitation (figure S4). The probability density distributions reveal distinct patterns of inter-model spread (represented by one standard deviation) in NBP anomalies under wet and dry conditions. In arid and semi-arid regions (figures 3(a) and (b)), wet conditions exhibit a noticeably heavier right tail, indicating that larger NBP deviations occur more frequently when moisture is sufficient. In contrast, in semi-humid and humid regions (figures 3(c) and (d)), dry conditions show a more extended tail and higher probability density for large NBP deviation values, suggesting stronger model divergence under water stress.

The Kolmogorov–Smirnov test confirms that these distributional differences between wet and dry conditions are statistically significant ($p < 0.001$). The accompanying boxplots further support this pattern: wet events in arid and semi-arid regions display higher medians and longer upper whiskers, whereas in semi-humid and humid regions, dry events correspond to higher medians and greater spread. Together, these results highlight that inter-model spread is more sensitive to wet anomalies in moisture-limited regions, but to drought-induced stress in energy-limited regions. When precipitation thresholds were applied to define wet and dry events, the results remained nearly identical to those described above (figure S5).

To further assess model performance, we present the mean NBP anomalies of individual models and the multi-model ensemble mean under wet and dry conditions across climate zones (figure 4). Under dry episodes, all models consistently simulate negative NBP anomalies, with the multi-model ensemble mean displaying the largest magnitude in humid regions. Notably, the magnitudes of anomalies from individual model diverge substantially, indicating the largest inter-model spread in humid regions. In contrast, under wet episodes, most models simulate an enhancement in carbon sinks (positive NBP anomalies) across all climate zones, albeit characterized by substantial inter-model differences. Some models, however, produce negative NBP anomalies under wet conditions, and these models vary by

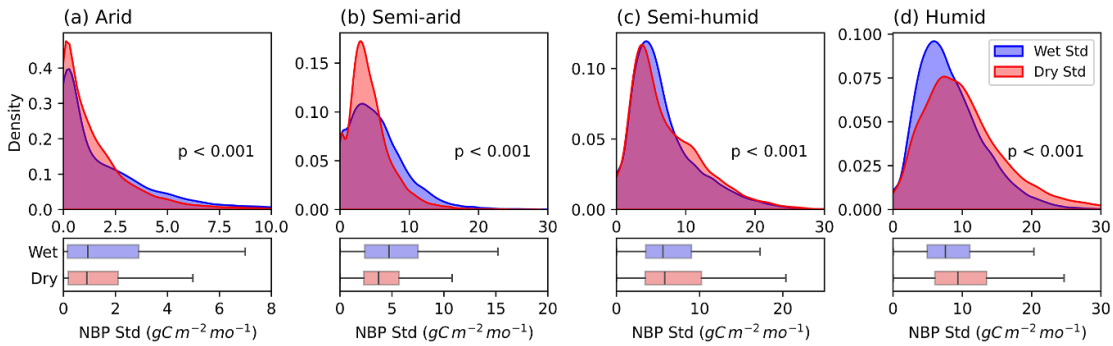

Figure 3. Density distributions and boxplots of inter-model spread across climate zones. Distributions are shown for (a) arid, (b) semi-arid, (c) semi-humid, and (d) humid regions under both wet and dry conditions. In the boxplots, the central line denotes the median, the box bounds represent the 25th and 75th percentiles, and the whiskers indicate the range of extreme values.

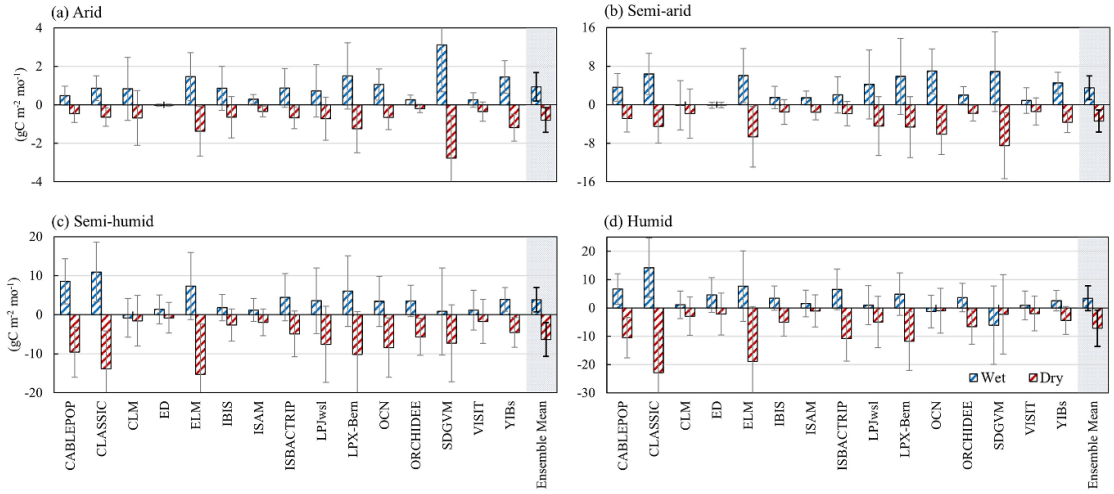

Figure 4. Mean NBP anomalies of individual models and multi-model ensemble mean under wet and dry conditions across climate zones. Panels show results for (a) arid, (b) semi-arid, (c) semi-humid, and (d) humid regions. For individual models, thin gray error bars denote ± 0.5 standard deviation (σ) across individual hydroclimatic events, representing inter-event variability. For the ensemble mean, thick black error bars signify ± 1 σ across the mean responses of all models, characterizing inter-model uncertainty.

region–for example, EDv3 in arid regions, CLM and EDv3 in semi-arid regions, CLM in semi-humid regions, and OCN and SDGVM in humid regions. However, precipitation-defined events more prominently highlight the impacts of hydroclimatic extremes on carbon sinks in semi-humid regions, with the largest positive and negative anomalies (figure S6).

Moreover, the magnitude of dry-induced anomalies generally exceeds that of wet-induced anomalies in semi-humid and humid regions, revealing an asymmetric response of NBP to hydroclimatic extremes (figures 4(c) and (d)). By contrast, in arid and semi-arid regions, the responses to wet and dry conditions are of comparable magnitude (figures 4(a) and (b)). The large inter-model discrepancies, including opposing NBP responses, highlight the persistent challenges faced by current TBMs in accurately capturing ecosystem responses to hydroclimatic extremes.

3.2.3. Uncertainties across biomes

To elucidate biome-dependent differences in inter-model variability, we categorized the global land surface into six major ecosystem types: grasslands, savannas, shrublands, tropical forests, extratropical forests, and croplands (figure S7). Overall, both the probability density distributions and boxplots consistently reveal that inter-model differences are significantly pronounced for grasslands, savannas, and shrublands under wet conditions, as evidenced by higher median values. In contrast, tropical forests, extratropical forests, and croplands exhibit greater inter-model divergence under dry conditions (figure 5). The Kolmogorov-Smirnov test confirms that these contrasts between wet and dry events are highly significant ($p < 0.001$). These findings are further supported by sensitivity analyses based on alternative event-selection criteria, with only minor discrepancies observed for savannas (figure S8).

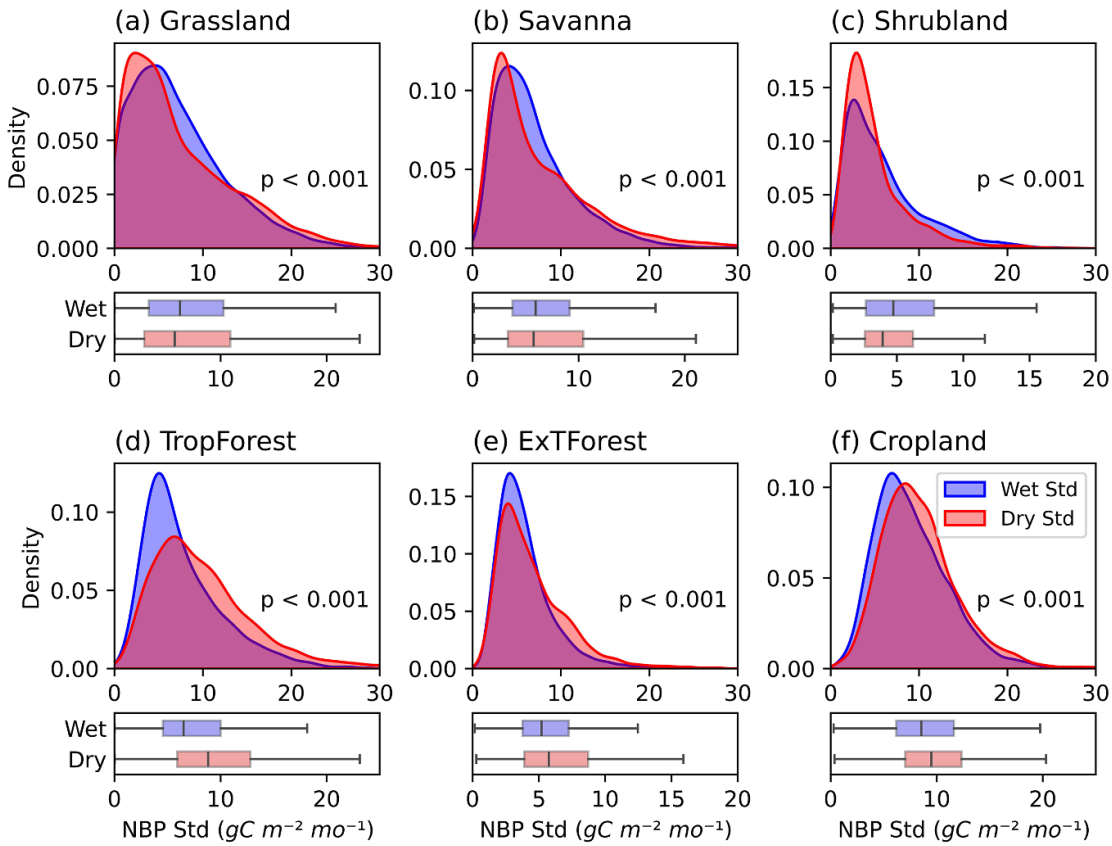

Figure 5. Density distributions and boxplots of inter-model spread across ecosystem types. Distributions are shown for (a) grassland, (b) savanna, (c) shrubland, (d) tropical forest, (e) extra tropical forest, and (f) cropland under both wet and dry conditions. In the boxplots, the central line denotes the median, the box bounds represent the 25th and 75th percentiles, and the whiskers indicate the range of extreme values.

When comparing mean NBP anomalies across individual models, considerable inter-model discrepancies are evident in grasslands under both wet and dry conditions, suggesting that current models still face challenges in accurately and consistently representing carbon flux responses in these ecosystems (figure S9). The robustness of this result is further validated by the precipitation-threshold screening, although the magnitude of the spread is slightly smaller (figure S10).

3.3. Biological mechanisms underlying inter-model uncertainties in NBP responses

Since NBP anomalies are largely driven by the combined effects of GPP and Reco, we further examined the uncertainties in simulated GPP and Reco responses to identify the dominant contributor to NBP uncertainty (figure 6). The spatial pattern of anomalous GPP closely resembles that of NBP but exhibits stronger intensity (figures 1 and S11). In contrast, anomalous Reco shows a more homogeneous response, with most regions exhibiting positive anomalies under wet conditions and negative anomalies under dry conditions (figure S12).

The spatial distributions of inter-model standard deviations for both GPP and Reco largely mirror those of NBP under both wet and dry conditions (figures 2 and 6). Across the majority of regions, GPP exhibits a larger inter-model spread than Reco; specifically, GPP standard deviations exceed those of Reco in 77% and 83% of grid cells under wet and dry events, respectively. Moreover, for both GPP and Reco, the regions with higher inter-model spread under dry conditions are slightly larger than those under wet conditions (figures 6(c) and (f)), consistent with results in NBP (figure 2(c)). Quantitative analysis of latitudinal averages further confirms the key role of GPP uncertainty, particularly in the low latitudes. Overall, the pronounced inter-model spreads in NBP responses to extreme hydroclimatic events primarily arise from uncertainties in simulating GPP, which are largely attributable to differences in model parameterizations and parameter values (Rogers 2014, Rogers *et al* 2014, Wang *et al* 2021).

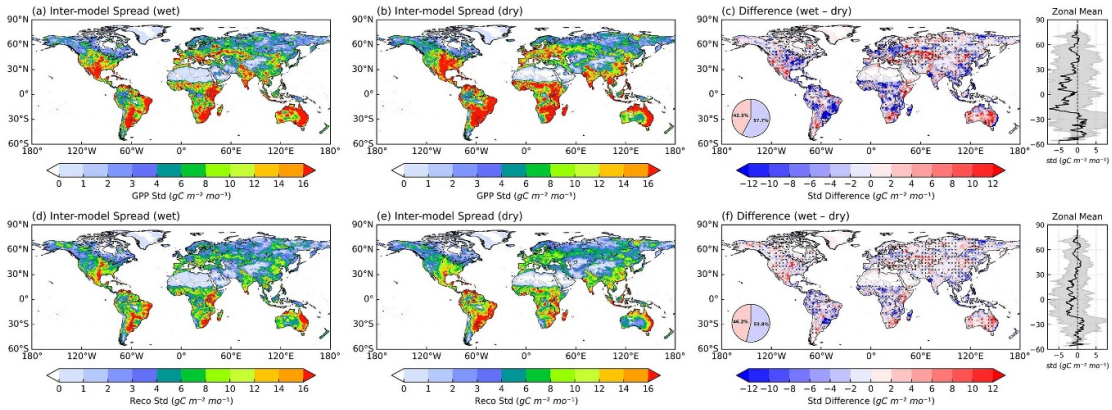

Figure 6. Inter-model spread of simulated GPP and Reco responses to hydroclimatic extremes. Panels (a), (b) and (d), (e) show the spatial distribution of standard deviations among TRENDY v12 models for GPP and Reco during wet and dry events, respectively. Panels (c) and (f) show the differences between wet and dry conditions, supplemented by the corresponding latitudinal averages. The inset pie charts demonstrate the percentage of vegetated areas exhibiting positive versus negative differences in spread. GPP and Reco are expressed in gC m^{-2} mo^{-1}. Regions marked with black dots indicate statistically significant differences based on Levene's test ($p < 0.05$).

4. Discussion

Although the multi-model ensemble mean reproduces the sign of terrestrial carbon flux responses to hydroclimatic extremes at approximately 60% of the study sites, the simulated magnitudes still deviate substantially from FLUXNET observations (figure 1). This agrees with Seiler *et al* (2022), who demonstrated that while TRENDY simulations capture the spatial patterns of GPP, NEE, and Reco, they often fail to replicate the amplitudes. Similarly, O'sullivan *et al* (2022) reported that dynamic global vegetation models (DGVMs) from TRENDY v10 provide consistent global land carbon sink estimates yet diverge significantly at regional scales. Our analysis indicates that such divergence persists across climate zones and vegetation types, where model responses vary in both magnitude and directionality (figures 4 and S9). Methodologically, the use of the Land-Use Harmonization 2 (LUH2-GCB) dataset across TRENDY models (Sitch *et al* 2024)—combined with the fact that most models incorporate multiple plant functional types within a single grid cell—may introduce discrepancies when compared against our site-specific IGBP-based analysis. Furthermore, arid and semi-arid regions have been identified as biogeochemical hotspots where precipitation extremes exert disproportionately strong effects on terrestrial carbon uptake (Pan *et al* 2020). However, our results highlight these regions as areas of high inter-model uncertainty during extreme events (figures 4(a) and (b)). These uncertainties primarily stem from divergent parameterizations of photosynthesis and respiration within current DGVMs (Lloyd and Taylor 1994, Grant *et al* 2003, Sitch *et al* 2008, Rogers 2014, Rogers *et al* 2014).

Peng *et al* (2024) identified an optimal soil-moisture threshold for GPP, suggesting that both relatively low and high soil moisture can suppress plant photosynthesis. Furthermore, low forest cover associated with higher drought thresholds implies weaker resistance (Li *et al* 2023), which aligns with anomalous carbon-source behavior in most non-forest regions during drought episodes (figure 1(f)). To date, most studies have emphasized drought stress based on field experiments (Ohlert *et al* 2025), EC measurements (Huang *et al* 2013) and model simulations (Zscheischler *et al* 2014b). However, DGVMs may overestimate drought impacts on vegetation owing to their inadequate representation of the nonlinear responses of plant growth to drought stress (Li *et al* 2023). This overstated sensitivity is often linked to the simplified representation of plant belowground traits; specifically, rooting depth serves as a critical regulator of carbon sink dynamics, as deeper roots allow plants to access deep-soil water and thus buffering the effects of short-term precipitation deficits (Sharma *et al* 2023). Most current models, however, employ static or oversimplified root profiles that fail to capture these adaptive buffering strategies. Consequently, many researchers seek to reduce uncertainty through process-based refinements and parameter optimization. For example, Eller *et al* (2020) introduced the xylem-hydraulic stomatal optimization model that simulates the drought-induced responses of leaf stomatal conductance in woody plants more accurately and parsimoniously. Additionally, ecosystem responses to extreme wet events remain poorly explored. Our results show that at mid-and high latitudes, inter-model uncertainties under wet conditions are comparable to or even exceed those under dry conditions (figure 2),

suggesting that wet extremes are a critical and underrepresented process in current TBMs. Unfortunately, most TBMs fail to represent the depressive effect of excessive soil water (Li *et al* 2023), potentially leading to systematic biases in NBP estimates. Excessive rainfall can induce oxygen limitation, nutrient leaching, and soil erosion, thereby constraining productivity and carbon turnover (Piao *et al* 2019). These mechanisms are rarely parameterized, leading to inconsistent simulations of wet-event responses. Model improvement should therefore incorporate hydrological and biogeochemical processes associated with waterlogging and saturation effects to better capture the full spectrum of hydroclimatic extremes. For instance, CROPR incorporates processes such as the waterlogging aeration factor, transpiration, and plant adaptation and recovery following waterlogging, thereby improving its capacity to capture yield penalties induced by waterlogging at different growth stages with greater fidelity (Liu *et al* 2020).

Under continued warming, the frequency and intensity of extreme precipitation are projected to increase, especially across mid-latitude and tropical regions (Collins *et al* 2013). Enhancing model fidelity in simulating wet-event impacts is thus essential for reliable projections of terrestrial carbon sink variability and for assessing the stability of ecosystem carbon dynamics under a changing climate.

5. Conclusion

In this study, we assessed the uncertainties in TRENDY model simulations of terrestrial carbon sink responses to hydroclimatic extremes from 1980 to 2022 by systematically comparing model outputs across diverse regions and event types. Our results indicate that the multi-model ensemble mean generally exhibits weaker anomalous responses than observations, though it captures the directionality of site-level NBP shifts at approximately 60% of stations. Notably, the models' capacity to replicate NBP variations is higher during dry events but degrades significantly under wet conditions. Spatially, under wet conditions, most regions acted as anomalous carbon sinks, except for high-latitude areas of the Northern Hemisphere (>50° N), the eastern United States, southeastern China, and southeastern South America; this pattern largely reverses during dry events.

The spatial pattern of inter-model spread revealed substantial heterogeneity under both hydroclimatic extremes. Zonal averages indicated that stronger inter-model spreads under dry events were mainly confined between 30° S and 30° N, whereas other latitudes showed comparable or even greater spreads under wet events. Overall, inter-model uncertainties were nearly balanced between wet and dry conditions, with 47.8% of vegetated areas exhibiting larger spreads under wet conditions and 52.2% under dry conditions.

We further found that inter-model spread was more sensitive to wet anomalies in arid and semi-arid regions, but to drought-induced stress in semi-humid and humid regions. Across biomes, inter-model uncertainties were substantially larger for grasslands, savannas, and shrublands under wet conditions, whereas tropical forests, extratropical forests, and croplands exhibited greater divergence under dry conditions. Finally, we demonstrated that the large inter-model spreads in NBP responses to hydroclimatic extremes primarily originated from uncertainties in simulating GPP.

Acknowledgments

We acknowledge the Global Carbon Project for coordinating the Global Carbon Budget and thank the land modelling groups for producing and sharing their model outputs. We extend special thanks to S. Sitch for organizing the TRENDY initiative. This work used eddy covariance data acquired and shared by the FLUXNET 2015. This research has been supported by the National Natural Science Foundation of China (Grant No. 42475129); the Tibet science and technology innovation base construction project (XZ202401YD0008); NASA Carbon Monitoring System (80NSSC21K1059); NASA GEDI Competed Science Team (8080NSSC24K0599) and NASA Early Career Investigator Program in Earth Science (80NSSC24K1632).

Data availability statement

The FLUXNET 2015 datasets are available at https://fluxnet.org/data/fluxnet2015-dataset/. The TRENDY v12 data are available at https://globalcarbonbudgetdata.org/. Land precipitation data from CRU v. 4.09 are available at https://crudata.uea.ac.uk/cru/data/hrg/. MCD12Q1 Version 6.1 data are available at https://lpdaac.usgs.gov/products/mcd12q1v061/.

Supplementary data 1 available at http://doi.org/10.1088/1748-9326/ae4b55/data1.

Conflict of interest

The authors declare no conflicts of interest related to this work.

ORCID iDs

Zishan Wang 0009-0006-0827-880X
Jun Wang 0000-0001-7359-1647
Benjamin Poulter 0000-0002-9493-8600
Gesa Meyer 0000-0003-3199-5250
George Hurtt 0000-0001-7278-202X

Hao Zhou 0000-0002-8888-4386
Lei Ma 0000-0002-3959-4155
Patrick C McGuire 0000-0001-6592-4966
Qing Sun 0000-0003-0767-4721
Wenping Yuan 0000-0002-1469-4395

References

Adams J 2017 Climate_indices, an open source Python library providing reference implementations of commonly used climate indices

Ahlström A *et al* 2015 The dominant role of semi-arid ecosystems in the trend and variability of the land CO_2 sink *Science* **348** 895–9

Asaadi A, Arora V K, Melton J R and Bartlett P 2018 An improved parameterization of leaf area index (LAI) seasonality in the Canadian Land Surface Scheme (CLASS) and Canadian Terrestrial Ecosystem Model (CTEM) modelling framework *Biogeosciences* **15** 6885–907

Burrows S M *et al* 2020 The DOE E3SM v1.1 biogeochemistry configuration: description and simulated ecosystem-climate responses to historical changes in forcing *J. Adv. Model. Earth Syst.* **12** e2019MS001766

Chen Z, Qian Z, Huang B, Feng G and Sun G 2025 Increased drought impacts on vegetation productivity in drylands under climate change *Geophys. Res. Lett.* **52** e2025GL115616

Collins M *et al* 2013 Long-term climate change: projections, commitments and irreversibility *Climate Change 2013-The Physical Science Basis: Contribution of Working Group I to the Fifth Assessment Report of the Intergovernmental Panel on Climate Change* (Cambridge University Press)

Dai L, Yang Y, Wang X, Yang G, Liang M and Hu Z 2024 Positive asymmetric responses indicate larger carbon sink with increase in precipitation variability in global terrestrial ecosystems *Innov. Geosci.* **2** 100060

Delire C *et al* 2020 The global land carbon cycle simulated with ISBA-CTRIP: improvements over the last decade *J. Adv. Model. Earth Syst.* **12** e2019MS001886

Eller C B *et al* 2020 Stomatal optimization based on xylem hydraulics (SOX) improves land surface model simulation of vegetation responses to climate *New Phytol.* **226** 1622–37

Fay P A, Blair J M, Smith M D, Nippert J B, Carlisle J D and Knapp A K 2011 Relative effects of precipitation variability and warming on tallgrass prairie ecosystem function *Biogeosciences* **8** 3053–68

Feldman A F, Feng X, Felton A J, Konings A G, Knapp A K, Biederman J A and Poulter B 2024 Plant responses to changing rainfall frequency and intensity *Nat. Rev. Earth Environ.* **5** 276–94

Friedl M and Sulla-Menashe D 2022 MODIS/Terra+ aqua land cover type yearly L3 global 500 m SIN grid V061, NASA EOSDIS land processes distributed active archive center

Friedlingstein P *et al* 2025 Global carbon budget 2024 *Earth Syst. Sci. Data* **17** 965–1039

Grant R F, Oechel W C and Ping C-L 2003 Modelling carbon balances of coastal arctic tundra under changing climate *Glob. Change Biol.* **9** 16–36

Haverd V, Smith B, Nieradzik L, Briggs P R, Woodgate W, Trudinger C M, Canadell J G and Cuntz M 2018 A new version of the CABLE land surface model (Subversion revision r4601) incorporating land use and land cover change, woody vegetation demography, and a novel optimisation-based approach to plant coordination of photosynthesis *Geosci. Model Dev.* **11** 2995–3026

He B *et al* 2022 Worldwide impacts of atmospheric vapor pressure deficit on the interannual variability of terrestrial carbon sinks *Natl Sci. Rev.* **9** nwab150

Huang H, Cui H and Ge Q 2021 Assessment of potential risks induced by increasing extreme precipitation under climate change *Nat. Hazards* **108** 2059–79

Huang K, Wang S, Zhou L, Wang H, Liu Y and Yang F 2013 Effects of drought and ice rain on potential productivity of a subtropical coniferous plantation from 2003 to 2010 based on eddy covariance flux observation *Environ. Res. Lett.* **8** 035021

Ito A and Inatomi M 2012 Use of a process-based model for assessing the methane budgets of global terrestrial ecosystems and evaluation of uncertainty *Biogeosciences* **9** 759–73

Jain A K, Meiyappan P, Song Y and House J I 2013 CO_2 emissions from land-use change affected more by nitrogen cycle, than by the choice of land-cover data *Glob. Change Biol.* **19** 2893–906

Jiao K, Liu Z, Wang W, Yu K, Mcgrath M J and Xu W 2024 Carbon cycle responses to climate change across China's terrestrial ecosystem: sensitivity and driving process *Sci. Total Environ.* **915** 915170053

Kato E, Kinoshita T, Ito A, Kawamiya M and Yamagata Y 2013 Evaluation of spatially explicit emission scenario of land-use change and biomass burning using a process-based biogeochemical model *J. Land Use Sci.* **8** 104–22

Krinner G, Viovy N, De Noblet-Ducoudré N, Ogée J, Polcher J, Friedlingstein P, Ciais P, Sitch S and Prentice I C 2005 A dynamic global vegetation model for studies of the coupled atmosphere-biosphere system *Glob. Biogeochem. Cycles* **19** GB1015

Lawrence D M *et al* 2019 The community land model version 5: description of new features, benchmarking, and impact of forcing uncertainty *J. Adv. Model. Earth Syst.* **11** 4245–87

Li X *et al* 2023 Global variations in critical drought thresholds that impact vegetation *Natl Sci. Rev.* **10** nwad049

Lienert S and Joos F 2018 A Bayesian ensemble data assimilation to constrain model parameters and land-use carbon emissions *Biogeosciences* **15** 2909–30

Liu K, Harrison M T, Shabala S, Meinke H, Ahmed I, Zhang Y, Tian X and Zhou M 2020 The state of the art in modeling waterlogging impacts on plants: what do we know and what do we need to know *Earth's Future* **8** e2020EF001801

Lloyd J and Taylor J A 1994 On the temperature dependence of soil respiration *Funct. Ecol.* **8** 315–23

Lloyd-Hughes B and Saunders M A 2002 A drought climatology for Europe *Int. J. Climatol.* **22** 1571–92

Loveland T R and Belward A S 1997 The IGBP-DIS global 1km land cover data set, DISCover: first results *Int. J. Remote Sens.* **18** 3289–95

Ma L *et al* 2022 Global evaluation of the ecosystem demography model (ED v3.0) *Geosci. Model Dev.* **15** 1971–94

Mckee T B, Doesken N J and Kleist J 1993 The relationship of drought frequency and duration to time scales *Proc. 8th Conf. on Applied Climatology* (*California*) pp 179–83

Meiyappan P, Jain A K and House J I 2015 Increased influence of nitrogen limitation on CO_2 emissions from future land use and land use change *Glob. Biogeochem. Cycles* **29** 1524–48

Melton J R, Arora V K, Wisernig-Cojoc E, Seiler C, Fortier M, Chan E and Teckentrup L 2020 CLASSIC v1.0: the open-source community successor to the Canadian Land Surface Scheme (CLASS) and the Canadian Terrestrial Ecosystem Model (CTEM)—part 1: model framework and site-level performance *Geosci. Model Dev.* **13** 2825–50

Moorcroft P R, Hurtt G C and Pacala S W 2001 A method for scaling vegetation dynamics: the ecosystem demography model (ED) *Ecol. Monogr.* **71** 557–86

O'sullivan M *et al* 2022 Process-oriented analysis of dominant sources of uncertainty in the land carbon sink *Nat. Commun.* **13** 4781

Ohlert T *et al* 2025 Drought intensity and duration interact to magnify losses in primary productivity *Science* **390** 284–9

Pan S *et al* 2020 Climate extreme versus carbon extreme: responses of terrestrial carbon fluxes to temperature and precipitation *J. Geophys. Res.-Biogeosci.* **125** e2019JG005252

Pastorello G *et al* 2020 The FLUXNET2015 dataset and the ONEFlux processing pipeline for eddy covariance data *Sci. Data* **7** 225

Peng J, Tang J, Xie S, Wang Y, Liao J, Chen C, Sun C, Mao J, Zhou Q and Niu S 2024 Evidence for the acclimation of ecosystem photosynthesis to soil moisture *Nat. Commun.* **15** 9795

Piao S, Zhang X, Chen A, Liu Q, Lian X, Wang X, Peng S and Wu X 2019 The impacts of climate extremes on the terrestrial carbon cycle: a review *Sci. China Earth Sci.* **62** 1551–63

Poulter B, Frank D C, Hodson E L and Zimmermann N E 2011 Impacts of land cover and climate data selection on understanding terrestrial carbon dynamics and the CO_2 airborne fraction *Biogeosciences* **8** 2027–36

Rhee J and Im J 2017 Meteorological drought forecasting for ungauged areas based on machine learning: using long-range climate forecast and remote sensing data *Agric. For. Meteorol.* **237–238** 105–22

Rogers A 2014 The use and misuse of $V_{c,max}$ in Earth System Models *Photosynth. Res.* **119** 15–29

Rogers A, Medlyn B E and Dukes J S 2014 Improving representation of photosynthesis in Earth System Models *New Phytol.* **204** 12–14

Seiler C *et al* 2022 Are terrestrial biosphere models fit for simulating the global land carbon sink? *J. Adv. Model. Earth Syst.* **14** e2021MS002946

Sharma B, Kumar J, Ganguly A R and Hoffman F M 2023 Carbon cycle extremes accelerate weakening of the land carbon sink in the late 21st century *Biogeosciences* **20** 1829–41

Shu S, Jain A K, Koven C D and Mishra U 2020 Estimation of permafrost SOC stock and turnover time using a land surface model with vertical heterogeneity of permafrost soils *Glob. Biogeochem. Cycles* **34** e2020GB006585

Sitch S *et al* 2008 Evaluation of the terrestrial carbon cycle, future plant geography and climate-carbon cycle feedbacks using five Dynamic Global Vegetation Models (DGVMs) *Glob. Change Biol.* **14** 2015–39

Sitch S *et al* 2015 Recent trends and drivers of regional sources and sinks of carbon dioxide *Biogeosciences* **12** 653–79

Sitch S *et al* 2024 Trends and drivers of terrestrial sources and sinks of carbon dioxide: an overview of the TRENDY project *Glob. Biogeochem. Cycles* **38** e2024GB008102

Steensen B M, Myhre G, Hodnebrog Ø and Fischer E 2025 Future increase in European compound events where droughts end in heavy precipitation *npj Clim. Atmos. Sci.* **8** 267

Thi N Q, Govind A, Le M-H, Linh N T, Anh T T M, Hai N K and Ha T V 2023 Spatiotemporal characterization of droughts and vegetation response in Northwest Africa from 1981 to 2020 *Egypt. J. Remote Sens. Space Sci.* **26** 393–401

Von Buttlar J *et al* 2018 Impacts of droughts and extreme-temperature events on gross primary production and ecosystem respiration: a systematic assessment across ecosystems and climate zones *Biogeosciences* **15** 1293–318

Vuichard N, Messina P, Luyssaert S, Guenet B, Zaehle S, Ghattas J, Bastrikov V and Peylin P 2019 Accounting for carbon and nitrogen interactions in the global terrestrial ecosystem model ORCHIDEE (trunk version, rev 4999): multi-scale evaluation of gross primary production *Geosci. Model Dev.* **12** 4751–79

Walker A P *et al* 2017 The impact of alternative trait-scaling hypotheses for the maximum photosynthetic carboxylation rate (V_{cmax}) on global gross primary production *New Phytol.* **215** 1370–86

Wang J *et al* 2018 Contrasting interannual atmospheric CO_2 variabilities and their terrestrial mechanisms for two types of El Niños *Atmos. Chem. Phys.* **18** 10333–45

Wang J *et al* 2023 Unprecedented decline in photosynthesis caused by summer 2022 record-breaking compound drought-heatwave over Yangtze River Basin *Sci. Bull.* **68** 2160–3

Wang J, Jiang F, Wang H, Qiu B, Wu M, He W, Ju W, Zhang Y, Chen J M and Zhou Y 2021 Constraining global terrestrial gross primary productivity in a global carbon assimilation system with OCO-2 chlorophyll fluorescence data *Agric. For. Meteorol.* **304–305** 108424

Wang Z, Wang J, Zhou H, Cai Q, Yan R, Wang H, Huang Z, Wang M and Ju W 2026 Loss and recovery of terrestrial carbon sinks induced by 2020 extreme precipitation in the Yangtze River Valley *J. Hydrol.* **664** 134390

Woodward F I and Lomas M R 2004 Vegetation dynamics—simulating responses to climatic change *Biol. Rev.* **79** 643–70

Xu X, Piao S, Wang X, Chen A, Ciais P and Myneni R B 2012 Spatio-temporal patterns of the area experiencing negative vegetation growth anomalies in China over the last three decades *Environ. Res. Lett.* **7** 035701

Yan R *et al* 2023 Interactive effects of the El Niño-Southern Oscillation and Indian Ocean Dipole on the tropical net ecosystem productivity *Agric. For. Meteorol.* **336** 109472

Yan R, Wang X, Wang J, Tan J and Ju W 2024 Warm early summer compensated reduction in photosynthesis caused by 2022 late summer extreme drought over the Tibetan Plateau *J. Geophys. Res.-Biogeosci.* **129** e2023JG007859

Yang X, Thornton P, Ricciuto D, Wang Y and Hoffman F 2023 Global evaluation of terrestrial biogeochemistry in the Energy Exascale Earth System Model (E3SM) and the role of the phosphorus cycle in the historical terrestrial carbon balance *Biogeosciences* **20** 2813–36

Yu G *et al* 2013 Spatial patterns and climate drivers of carbon fluxes in terrestrial ecosystems of China *Glob. Change Biol.* **19** 798–810

Yuan W *et al* 2014 Multiyear precipitation reduction strongly decreases carbon uptake over northern China *J. Geophys. Res.-Biogeosci.* **119** 881–896

Yue X and Unger N 2015 The Yale Interactive terrestrial Biosphere model version 1.0: description, evaluation and implementation into NASA GISS ModelE2 *Geosci. Model Dev.* **8** 2399–417

Zaehle S, Ciais P, Friend A D and Prieur V 2011 Carbon benefits of anthropogenic reactive nitrogen offset by nitrous oxide emissions *Nat. Geosci.* **4** 601–5

Zaehle S and Friend A D 2010 Carbon and nitrogen cycle dynamics in the O-CN land surface model: 1. Model description, site-scale evaluation, and sensitivity to parameter estimates *Glob. Biogeochem. Cycles* **24** GB1005

Zeppel M J B, Wilks J V and Lewis J D 2014 Impacts of extreme precipitation and seasonal changes in precipitation on plants *Biogeosciences* **11** 3083–93

Zhang G, Wang Y, Sun J, Chu S, Zhang B, Duan L and Liu T 2025 Exploring the response of net ecosystem CO_2 exchange to precipitation events in a wet meadow ecosystem by using an improved semi-empirical physical model *J. Hydrol.* **660** 133398

Zscheischler J *et al* 2014a A few extreme events dominate global interannual variability in gross primary production *Environ. Res. Lett.* **9** 035001

Zscheischler J *et al* 2014b Impact of large-scale climate extremes on biospheric carbon fluxes: an intercomparison based on MsTMIP data *Glob. Biogeochem. Cycles* **28** 585–600